

Terahertz radiation by two-color lasers due to the field ionization of gasesWei-Min Wang,^{1,*} Yu-Tong Li,¹ Zheng-Ming Sheng,^{1,2,3,†} Xin Lu,¹ and Jie Zhang^{1,2}¹*Beijing National Laboratory for Condensed Matter Physics, Institute of Physics, CAS, Beijing 100190, China*²*Key Laboratory for Laser Plasmas (Ministry of Education) and Department of Physics, Shanghai Jiao Tong University, Shanghai 200240, China*³*Department of Mathematics, Institute of Natural Sciences, and MOE-LSC, Shanghai Jiao Tong University, Shanghai 200240, China*

(Received 8 November 2012; published 26 March 2013)

Terahertz (THz) radiation via the two-color laser scheme is investigated theoretically and numerically when the second laser is at different harmonic orders of the main laser. It is found that THz radiation can be generated only when the second laser is an even harmonic and the THz field strength does not show a simple scaling with the two laser amplitudes, suggesting that this is different from normal optical rectification or frequency mixing processes. The THz strength generally tends to decrease with increase of the even harmonic order. The strength is also sensitive to the carrier envelope (CE) phases of both the laser pulses even if their durations are quite long. With different CE phases, the strength can be proportional to either the sine or cosine of the relative phase displacement of the two lasers. For a given gas target except hydrogen, it increases with the laser amplitude between several saturation plateaus, each corresponding to a different ionization level. For a given main laser intensity, there is an optimized intensity of the second laser for the strongest THz radiation.

DOI: [10.1103/PhysRevE.87.033108](https://doi.org/10.1103/PhysRevE.87.033108)

PACS number(s): 52.59.Ye, 52.25.Jm, 42.72.Ai, 52.65.Rr

I. INTRODUCTION

Recently there is significant interest in generating strong terahertz (THz) waves with field strengths of MV/cm and above as required for nonlinear THz spectroscopies and THz nonlinear physics. Such THz waves are usually achieved through some accelerator-based method with the consequent limits of the bandwidth, wave form, and availability to most users. Another possible approach is based on large-aperture photoconductors, which can produce THz radiation with strength up to hundreds of kV/cm [1,2]. However, it is difficult to further enhance the THz strength because the photoconductors are limited by the material damage threshold and cannot bear too high pump fields. Plasma, without such a damage threshold, is proposed to be used as a new medium for powerful THz radiation sources driven by quite high pump fields. The feasibility of using plasma has been demonstrated in many experimental and theoretical investigations [3–33]. For example, THz radiation with energy up to 50 mJ/sr has been observed when a relativistic intense laser pulse irradiated a solid target, and was attributed to formation of a net current along the target surface [8]. Similar experimental demonstrations with solid plasma can be found in Refs. [3–7]. Such THz radiation has high energy and is broadband, but large divergence. Directed THz radiation was observed to be generated from a gas plasma via transition radiation at a plasma-vacuum boundary using an electron beam from a laser wakefield accelerator (LWFA) [9]. This scheme demands an ultrashort, ultraintense laser pulse ($\gtrsim 10^{19}$ W/cm²) and proper plasma density to first trigger the LWFA, and the THz emission direction is sensitive to the beam and plasma parameters. Via the two-color laser scheme with a fundamental or main laser mixed with its second harmonic in gases, THz emission along the laser propagation direction has been experimentally illustrated [10–14,20,21]. Such THz

radiation has a near single-cycle wave form with the central frequency at the plasma oscillation frequency [16–19]. So far, a field strength more than 400 kV/cm [12] has been experimentally achieved via the two-color laser scheme. This scheme has the potential to generate even more powerful THz radiation with field strength of MV/cm and above. A few other schemes based on gas plasmas have also been proposed, such as the linear mode conversion scheme with an ultraintense laser which drives wakefields in an inhomogeneous underdense plasma [24–28], the Cherenkov-like emission scheme with an intense laser in a plasma-gas channel [29,30], the bias electric field scheme in plasmas [31,32], and the mid-infrared laser scheme in gases [33].

Despite considerable investigation into the two-color scheme in both theory and experiment since it was proposed in 2000 by Cook and Hochstrasser [10], there are still many problems to be clarified with this scheme. First, there are two inconsistent experimental results reported on the dependence of the THz strength on the relative phase difference between the two laser pulses: one shows sine dependence [11,14] and the other cosine dependence [13]. Second, the THz intensity scaling shows a monotonic increase with the growing laser intensity or energy in some experiments [10–13], while it shows saturation in some other experiments [14]. Other issues to be clarified include the following: How can the energy conversion efficiency of the THz radiation be increased by choice of the intensities of the two-color lasers? What are the effects of different gas species on the THz generation and which gas can produce stronger THz radiation as well as higher conversion efficiency? Can the two-color laser scheme be extended to use other orders of harmonics in addition to the second harmonic?

We will clarify these problems through particle-in-cell (PIC) simulations with the field ionization of atoms included as well as the ionization current model, which was proposed in Refs. [11,14,15] and developed in Refs. [16–19]. The outline of the paper is as follows. In Sec. II, THz generation is analyzed with the second laser pulse at arbitrary harmonic order. The

*hbwwm1@iphy.ac.cn

†zmsheng@sjtu.edu.cn

THz strength dependence on the relative phase displacement is also investigated. The dependence is extended to the case with any carrier envelope (CE) phases of the two laser pulses in Sec. III. Then the THz intensity versus the main laser intensity is studied with various gas species in Sec. IV. The conversion efficiency is also discussed in this section. In Sec. V, the effects of the second laser intensity are analyzed. The THz saturation strengths at different intensity ratios are presented in Sec. VI. The paper concludes with a summary in Sec. VII.

II. EFFECT OF THE FREQUENCY AND INITIAL PHASE OF THE SECOND LASER

We first recall the THz generation mechanism of the two-color laser scheme described by the field ionization current model [14–16]. First, the second harmonic laser breaks the symmetry of the fundamental laser ionization in a gas and forms a transverse net current in the gas plasma [14–16], which can be clearly seen in PIC simulations [16]. Then the net current formed in the plasma is converted into THz radiation at the electron plasma frequency ω_p through the plasma dynamics [16–18], where $\omega_p = \sqrt{4\pi e^2 n_e / m_e}$ and n_e is the plasma electron density. The field strength of such THz radiation is proportional to both the net current strength and ω_p [16–18].

Then we analyze the net current production when the second laser frequency is at a certain harmonic order of the main laser. For simplicity, the one-dimensional (1D) case is considered, i.e., the two laser pulses are taken as plane waves. We consider laser pulses with durations far longer than the main laser cycle and therefore the longitudinal profiles of the pulses can be ignored in our analysis. Take the electric fields of the two laser pulses as $E = a_0 \sin[\omega_0(t - x/c)] + a_2 \sin[\omega_2(t - x/c) + \theta]$, where c is the light speed in the vacuum, a_0 the amplitude of the main laser, ω_0 its frequency, a_2 the amplitude of the second laser, ω_2 its frequency, and θ the relative phase. Here we assume that the gas density is low enough that the phase velocities of the lasers can be approximated by c . Consider that the second laser is a harmonic of the main laser and hence the properties of E can be obtained only by analyzing one cycle of the main laser. Set $\psi = \omega_0(t - x/c)$ and then the electric fields can be rewritten as

$$E = a_0 \sin(\psi) + a_2 \sin(m\psi + \theta), \quad (1)$$

where $m = \omega_2/\omega_0$ is an integer. The vector potential is given by

$$A = a_0 \cos(\psi) + \frac{a_2}{m} \cos(m\psi + \theta), \quad (2)$$

where A is normalized by $m_e c^2 / e$ and E by $m_e c \omega_0 / e$. According to Refs. [16–18], an electron created by laser field ionization gains a net transverse velocity $v_\perp / c = -A(\psi_0)$ after the passage of the laser pulses, where ψ_0 is the initial position or phase of the electron. Generally ψ_0 is around the extremum of E at which the ionization occurs with the highest probability. We then study the values of A at extrema of E , since the THz amplitude scales linearly with v_\perp or $A(\psi_0)$ [16]. It is clear that the THz wave amplitude depends on a linear combination of the two drive laser amplitudes as well as their relative phases, which cannot be described by standard nonlinear optical theory as normal optical rectification or frequency mixing processes.

Any extremum of E appears where the first order derivative of E is equal to zero, i.e.,

$$\frac{\partial E}{\partial \psi} = a_0 \cos(\psi) + m a_2 \cos(m\psi + \theta) = 0. \quad (3)$$

The second order derivative of E is given by

$$\frac{\partial^2 E}{\partial \psi^2} = -a_0 \sin(\psi) - m^2 a_2 \sin(m\psi + \theta). \quad (4)$$

When $\partial^2 E / \partial \psi^2 > 0$, the extremum is a maximum. Otherwise, the extremum is a minimum for $\partial^2 E / \partial \psi^2 < 0$.

In the following, we will first prove that no THz radiation can be generated when the second laser is an odd harmonic of the main laser. We then will show that THz radiation can be efficiently generated when the second laser is an even harmonic, according to Eqs. (1)–(4). It should be emphasized that the following analysis and simulations have nothing to do with a nonlinear optic effect of the medium. On the contrary, the THz generation depends on only the linear superposition of the two laser fields as expressed by Eqs. (1) and (2).

A. The second laser at an odd harmonic frequency

Assume that $\partial E / \partial \psi = 0$ at $\psi = \psi_0$. When $m = \omega_2/\omega_0$ is an odd number, one can easily prove that

$$\begin{aligned} \frac{\partial E}{\partial \psi}(\psi_0 + \pi) &= -\frac{\partial E}{\partial \psi}(\psi_0) = 0, \\ E(\psi_0 + \pi) &= -E(\psi_0), \\ A(\psi_0 + \pi) &= -A(\psi_0), \\ \frac{\partial^2 E}{\partial \psi^2}(\psi_0 + \pi) &= -\frac{\partial^2 E}{\partial \psi^2}(\psi_0). \end{aligned} \quad (5)$$

Equation (5) indicates that if a maximum or minimum of E appears at ψ_0 , there must be a minimum or maximum at $\psi_0 + \pi$; the maximum and minimum have the same absolute value; and the values of A at ψ_0 and $\psi_0 + \pi$ are opposite. This is clearly illustrated by Fig. 1. Therefore, if a group of electrons are created at ψ_0 , there must be another group of the same number of electrons created at $\psi_0 + \pi$. The

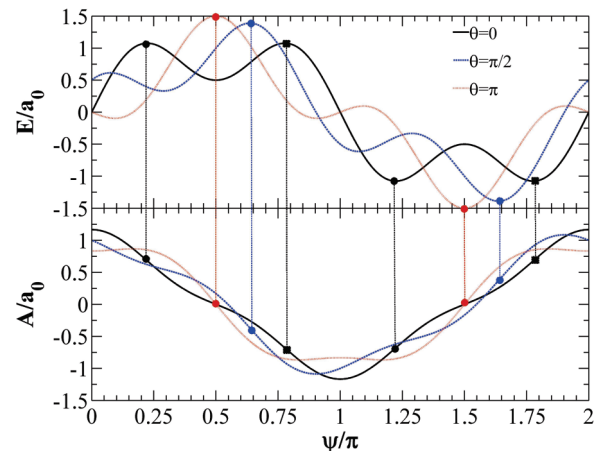


FIG. 1. (Color online) Numerical calculations of Eqs. (1) and (2) with different θ , where $\omega_2 = 3\omega_0$ and $a_2 = 0.5a_0$. The solid circles and squares mark the maxima and minima of the electric field E of the mixed lasers and the corresponding values of A .

two groups of electrons have opposite net velocities because $A(\psi_0 + \pi) = -A(\psi_0)$. Thus, the two net currents formed by the two groups of electrons can completely counteract each other and consequently no THz radiation is generated. This prediction is well verified by our PIC simulations with $m = 1, 3, 5,$ and 7 . One can see the parameters of the gases and laser pulses used in our PIC simulations in the Appendix.

B. The second laser at an even harmonic frequency

When m is an even number, Eq. (5) does not hold any longer. One can obtain

$$\frac{\partial E}{\partial \psi}(\psi_0 + \pi) = -a_0 \cos(\psi_0) + ma_2 \cos(m\psi_0 + \theta). \quad (6)$$

Usually $\frac{\partial E}{\partial \psi}(\psi_0 + \pi) \neq \frac{\partial E}{\partial \psi}(\psi_0)$, unless $\cos(\psi_0) = 0$. With $\cos(\psi_0) = 0$ and $\frac{\partial E}{\partial \psi}(\psi_0) = 0$, we derive $\psi_0 = \pi/2$ or $3\pi/2$ and $\theta = \pi/2$ or $3\pi/2$, where we consider ψ_0 and θ only within $[0, 2\pi]$ since $E, A, \partial E/\partial \psi$, and $\partial^2 E/\partial \psi^2$ are periodic functions with the period of 2π . Hence, when θ is taken as $\pi/2$ or $3\pi/2$, there are two extrema of E at $\psi_0 = \pi/2$ and $3\pi/2$, respectively. In this case, $A(\psi_0) = A(\psi_0 + \pi) = 0$. As a result, electrons created at the two extrema cannot gain net velocities. This suggests that THz radiation generation is inefficient when $\theta = \pi/2$ or $3\pi/2$.

When $m = 4n + 2$ (n is an integer), $E(\theta = \pi/2, \psi_0 = \pi/2) = a_0 - a_2$ and $E(\theta = \pi/2, \psi_0 = 3\pi/2) = -a_0 - a_2$; $E(\theta = 3\pi/2, \psi_0 = \pi/2) = a_0 + a_2$ and $E(\theta = 3\pi/2, \psi_0 = 3\pi/2) = -a_0 + a_2$. When $m = 4n$, $E(\theta = \pi/2, \psi_0 = \pi/2) = a_0 + a_2$ and $E(\theta = \pi/2, \psi_0 = 3\pi/2) = -a_0 + a_2$; $E(\theta = 3\pi/2, \psi_0 = \pi/2) = a_0 - a_2$ and $E(\theta = 3\pi/2, \psi_0 = 3\pi/2) = -a_0 - a_2$. Between the two extrema at $\psi_0 = \pi/2$ and $3\pi/2$, one of the absolute values of E is larger than the other. Usually ionization occurs only at the larger one. These properties can also be seen from Figs. 2, 3, 5(b), 5(e), and 5(g).

When θ is not taken as $\pi/2$ or $3\pi/2$, $\frac{\partial E}{\partial \psi}(\psi_0 + \pi) \neq \frac{\partial E}{\partial \psi}(\psi_0)$ and $\frac{\partial E}{\partial \psi}(\psi_0) = 0$. This indicates that THz radiation may be efficiently generated with an even number m , unlike the case

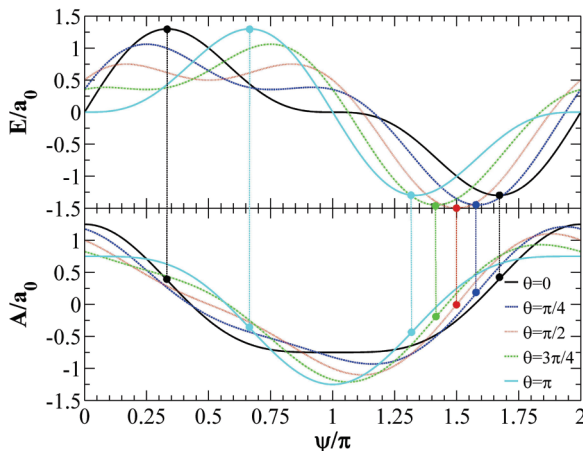


FIG. 2. (Color online) Numerical calculations of Eqs. (1) and (2) with different θ , where $\omega_2 = 2\omega_0$ and $a_2 = 0.5a_0$. The solid circles mark the maxima and minima of the electric field E of the mixed lasers and the corresponding values of A .

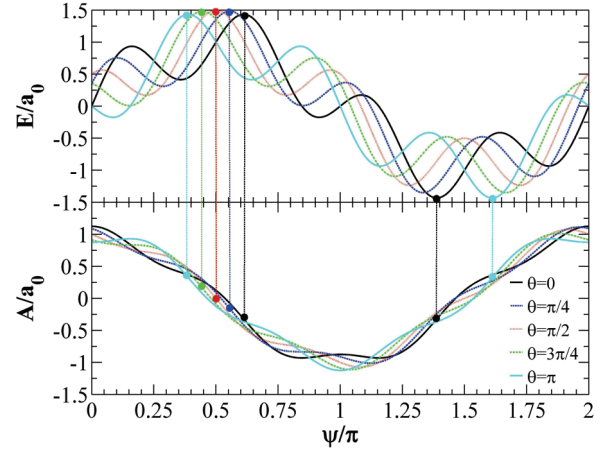


FIG. 3. (Color online) Numerical calculations of Eqs. (1) and (2) with different θ , where $\omega_2 = 4\omega_0$ and $a_2 = 0.5a_0$. The solid circles mark the maxima and minima of the electric field E of the mixed lasers and the corresponding values of A .

with an odd number m . To show it, we first consider two special cases with $\theta = 0$ and π , since the problem is difficult to analyze for other θ values. When $\theta = 0$ or π , one can prove that $E(2\pi - \psi) = -E(\psi)$, $A(2\pi - \psi) = A(\psi)$, $\frac{\partial E}{\partial \psi}(2\pi - \psi) = \frac{\partial E}{\partial \psi}(\psi)$, and $\frac{\partial^2 E}{\partial \psi^2}(2\pi - \psi) = -\frac{\partial^2 E}{\partial \psi^2}(\psi)$. Therefore, if a maximum of E appears at ψ_0 , there must be a minimum at $2\pi - \psi_0$. Ionization will occur at the two points with the same probability. At the two points, two net currents with the same direction and strength are formed since $A(2\pi - \psi_0) = A(\psi_0) \neq 0$ [$A(\psi_0) \neq \frac{\partial E}{\partial \psi}(\psi_0)$ and $\frac{\partial E}{\partial \psi}(\psi_0) = 0$]. This suggests that THz radiation can be efficiently generated.

In the following, we discuss the dependence of $A(\psi_0)$ (or THz generation) on θ . According to $\frac{\partial E}{\partial \psi}(\psi_0) = 0$, $A(\psi_0)$ is given by

$$A(\psi_0) = a_0 \left(1 - \frac{1}{m^2}\right) \cos(\psi_0), \quad (7)$$

where ψ_0 is a function of θ . Taking the derivative of $\frac{\partial E}{\partial \psi}(\psi_0) = 0$ with respect to θ , one derives

$$\frac{\partial \psi_0}{\partial \theta} = \frac{ma_2 \sin(m\psi_0 + \theta)}{\partial^2 E(\psi_0)/\partial \psi^2}. \quad (8)$$

We are interested in the case with $\sin(m\psi_0 + \theta) \sin(\psi_0) > 0$, where the main laser is strengthened by the second one at the extreme point ψ_0 . Under this condition, one can obtain

$$-\frac{1}{m} < \frac{\partial \psi_0}{\partial \theta} < 0. \quad (9)$$

According to the discussion presented above, when $m = 4n + 2$ and $\theta = \pi/2$, a minimum appears at $\psi_0 = 3\pi/2$, which satisfies $\sin(m\psi_0 + \theta) \sin(\psi_0) > 0$. Using Eqs. (9) and (7), one gets that as θ decreases from $\pi/2$ to 0 , ψ_0 is increased monotonically from $3\pi/2$ to a value smaller than 2π and consequently $A(\psi_0)$ is growing monotonically from 0 (see Fig. 2). As θ increases from $\pi/2$ to π , ψ_0 decreases monotonically from $3\pi/2$ to a value larger than π and thus $A(\psi_0)$ is reduced monotonically from 0 (see Fig. 2). That is, $A(\psi_0)$ decreases monotonically from $\theta = 0$ to π . It can

also be shown that $A(\psi_0)$ grows monotonically from $\theta = \pi$ to 2π [here ψ_0 is around $\pi/2$ and $A(\psi_0 = \pi/2, \theta = 3\pi/2) = 0$], through

$$\begin{aligned} \frac{\partial E}{\partial \psi}(\psi - \pi, \theta + \pi) &= -\frac{\partial E}{\partial \psi}(\psi, \theta), \\ E(\psi - \pi, \theta + \pi) &= -E(\psi, \theta), \\ A(\psi - \pi, \theta + \pi) &= -A(\psi, \theta), \\ \frac{\partial^2 E}{\partial \psi^2}(\psi - \pi, \theta + \pi) &= -\frac{\partial^2 E}{\partial \psi^2}(\psi, \theta). \end{aligned} \quad (10)$$

In the main laser cycle, the extrema of $|E|$ appear twice for $\theta = 0$ and π and once for other values of θ . When m is small (e.g., $m = 2$; see Fig. 2), the largest $|E|$ is much larger than the others. Thus, ionization usually occurs only at these points (two points for $\theta = 0$ and π and one point for the other θ). Thus THz generation is determined by $A(\psi_0)$ only at these points. According to Refs. [16–18], the scaling of the THz electric field strength is given by

$$E_{\text{THz}} \propto -A(\psi_0)\omega_p. \quad (11)$$

Note that to get Eq. (11) we have assumed that the number of electrons produced in a laser cycle does not vary with θ , since the total number of electrons created is nearly the same for different θ . In terms of the dependence of $A(\psi_0)$ on θ presented previously, one can obtain the THz strength dependence on θ for a small m ($m = 4n + 2$). The strongest THz radiation appears at $\theta = 0$ and π and the weakest THz radiation at $\theta = \pi/2$ and $3\pi/2$. This is verified by our PIC simulation results, as shown by the curves with $\omega_2 = 2\omega_0$ and $6\omega_0$ in Fig. 4. The parameters and setup of our PIC simulations can be seen in the Appendix.

The positions of the laser field ionization are also in good agreement with the previous predictions, as seen in Fig. 5. When $m = 2$, the ionization occurs only at 0.75 of the laser period for $\theta = \pi/2$ [see Fig. 5(b)]; for $\theta = 0$ the ionization

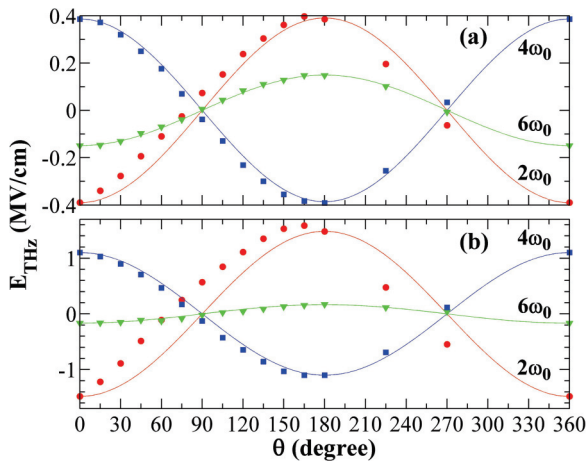


FIG. 4. (Color online) Amplitudes of THz electric fields versus the relative phases of the second lasers with different frequencies. The circular, square, and triangular points show PIC simulation results and the solid lines are cosine curves. The intensities of the main lasers are taken as 10^{14} W/cm² in (a) and 10^{15} W/cm² in (b). The second laser intensities are taken to be 25% of that of the main laser.

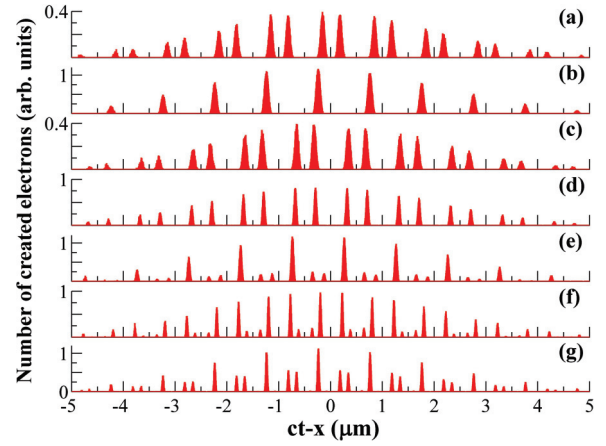


FIG. 5. (Color online) Number distributions of newly created electrons from field ionization vs $ct - x$. We take the second lasers with $\omega_2 = 2\omega_0$ and $\theta = 0$ in (a); $\omega_2 = 2\omega_0$ and $\theta = \pi/2$ in (b); $\omega_2 = 2\omega_0$ and $\theta = \pi$ in (c); $\omega_2 = 4\omega_0$ and $\theta = 0$ in (d); $\omega_2 = 4\omega_0$ and $\theta = \pi/2$ in (e); $\omega_2 = 6\omega_0$ and $\theta = 0$ in (f); and $\omega_2 = 6\omega_0$ and $\theta = \pi/2$ in (g). The intensities of the main lasers are fixed as 10^{14} W/cm². The second laser intensities are taken to be 25% of that of the main laser.

occurs twice at two symmetric points and the one within the range of laser period 0.5–1 is at the right of 0.75 of the laser period [see Fig. 5(a)]; for $\theta = \pi$ the ionization occurs twice symmetrically [see Fig. 5(c)]. When $m = 6$, the results are similar [see Figs. 5(f) and 5(g)] except that weak ionization occurs where the values of $|E|$ are slightly smaller than the largest one. With the growth of m , the number of ionization points will increase and therefore the dependence of THz generation on θ will become difficult to analyze. Generally, one expects that the THz radiation is weakened with increasing m because the ionization can occur at many points where the sign and the magnitude of $A(\psi_0)$ vary continuously. One observes in Fig. 4 that the THz radiation with $\omega_2 = 6\omega_0$ is weaker than that with $\omega_2 = 2\omega_0$ (one also sees the comparison between $\omega_2 = 4\omega_0$ and $\omega_2 = 2\omega_0$ in Figs. 4 and 6 below). Actually, our simulations show that as ω_2 is increased to $8\omega_0$ and $10\omega_0$, the THz radiation is gradually attenuated to noise level.

A similar result can be obtained for $m = 4n$ in the same way presented above. Using Eqs. (7), (9), and (10) and the maximum at $\psi_0 = \pi/2$ for $\theta = \pi/2$, one obtains that $A(\psi_0)$ grows monotonically from $\theta = \pi$ to 2π (see Fig. 3). In terms of Eq. (11), for a small m , the THz field strength (with sign) is reduced monotonically from $\theta = 0$ to π and grows monotonically from $\theta = \pi$ to 2π , where the strongest THz radiation appears at $\theta = 0$ and π and the weakest at $\theta = \pi/2$ and $3\pi/2$. This agrees with the PIC simulation results shown in the curves with $\omega_2 = 4\omega_0$ in Fig. 4.

Notice that in Fig. 4 the θ dependence approaches $(-1)^{m/2} \cos(\theta)$, i.e., $-\cos(\theta)$ for $m = 4n + 2$ and $\cos(\theta)$ for $m = 4n$. This can be attributed partially to the fact that $A(\psi_0)$ is a cosine function of ψ_0 and the latter varies monotonically with θ according to Eqs. (7) and (9). However, the exact dependence is difficult to derive analytically since $\partial\psi_0/\partial\theta$ expressed by Eq. (8) is complex.

III. EFFECT OF CARRIER ENVELOPE PHASES OF THE TWO-COLOR LASERS

There are three experimental results about the dependence of THz strength on θ , where $m = 2$ was taken. Two of them show $\sin(\theta)$ dependence [11,14] and the other shows $\cos(\theta)$ dependence [13]. Although these results look inconsistent, we shall show that both of them are possible. The reason is that the θ dependence varies with the CE phases of the two lasers even if the pulse durations are far longer than the main laser cycle, as shown in the following.

We have taken $E = a_0 \sin(\psi) + a_2 \sin(m\psi + \theta)$ in the previous analysis and simulations and obtained that the THz strength is proportional to $(-1)^{m/2} \cos(\theta)$. The dependence is changed to $-\sin(\theta')$, if the electric field is taken as $E' = a_0 \cos(\psi) + a_2 \cos(m\psi + \theta')$. This can be proved in terms of $E'(\psi - \pi/2) = E(\psi)$ and $A'(\psi - \pi/2) = A(\psi)$ by setting $\theta' = \theta + \pi(m - 1)/2$, where we have applied the displacement property of a periodic function, i.e., $E'(\psi - \pi/2)$ is equivalent to $E'(\psi)$. Therefore, either the sine or cosine dependence observed in experiments is possible since the CE phases of the two laser pulses are not clear in the experiments.

The dependence of the THz strength on the CE phases provides a robust tool for detecting the CE phases of the two laser pulses even with durations far longer than a cycle. Generally, the laser fields can be taken as $E = a_0 \sin(\psi + \psi_{CE1}) + a_2 \sin(m\psi + \psi_{CE2} + \theta)$, where ψ_{CE1} is the CE phase of the main laser and ψ_{CE2} is the CE phase of the second one. By use of the equivalence between $E(\psi)$ and $E(\psi - \psi_{CE1}) = a_0 \sin(\psi) + a_2 \sin(m\psi + \psi_{CE2} - m\psi_{CE1} + \theta)$, one can achieve that the THz strength

$$E_{\text{THz}} \propto (-1)^{m/2} \cos(\psi_{CE2} - m\psi_{CE1} + \theta). \quad (12)$$

Providing the minimum strength of the THz radiation is detected at θ_{\min} and the maximum detected at θ_{\max} , one can get ψ_{CE1} and ψ_{CE2} through $\psi_{CE2} - m\psi_{CE1} + \theta_{\min} = 0$ and $\psi_{CE2} - m\psi_{CE1} + \theta_{\max} = \pi$, where $m = 4n + 2$ is employed. For $m = 4n$, $\psi_{CE2} - m\psi_{CE1} + \theta_{\max} = 0$ and $\psi_{CE2} - m\psi_{CE1} + \theta_{\min} = \pi$.

In the following sections, we take the laser fields as Eq. (1) with $\theta = 0$ and $\omega_2 = 2\omega_0$ unless otherwise specified, which is favorable for THz generation according to previous analysis. We take the second laser intensity as 25% of the main laser intensity in our simulations in Sec. IV and change the second laser intensity to discuss its effect on THz generation in Sec. V.

IV. EFFECTS OF THE MAIN LASER INTENSITY AND GAS SPECIES

In this section, we will investigate the effect of the main laser intensity I_0 on THz generation and energy conversion. When a gas is not completely ionized, $A(\psi_0) \propto \sqrt{I_0}$ and ω_p or $\sqrt{n_e}$ grows monotonically with I_0 . According to Eq. (11), the THz intensity increases monotonically with I_0 , although it has a complex dependence on I_0 due to the complex dependence of $\sqrt{n_e}$ on I_0 . The monotonic increase of the THz intensity with the laser intensity has been observed in experiments employing low-intensity laser pulses in air [10–14]. This is also reproduced by our PIC simulations with hydrogen, helium, and nitrogen gases, as shown in Figs. 6(a), 7(a),

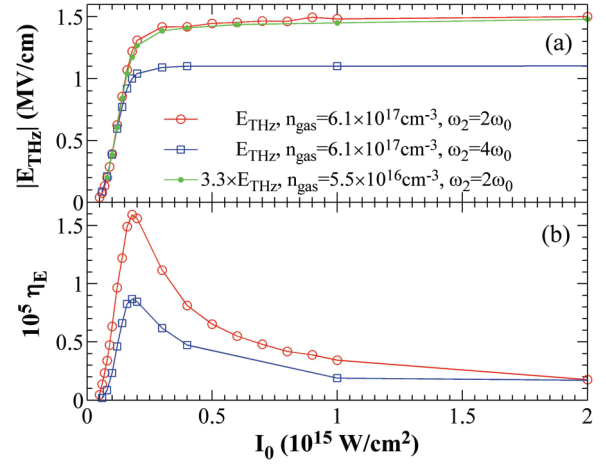


FIG. 6. (Color online) (a) Amplitudes of THz electric fields versus intensities of the main lasers. (b) Energy conversion efficiencies of THz radiation versus intensities of the main lasers. Different curves correspond to different hydrogen gas densities and different frequencies of the second laser in each plot.

and 8(a), respectively, for relatively low laser intensities. When the intensities are increased up to some thresholds, saturation is observed clearly in Figs. 6(a), 7(a), and 8(a), which has also been seen in the experiments in Ref. [14]. This saturation can be explained by Fig. 9. For low laser intensity, e.g., 10^{14} W/cm² used in Figs. 9(a) and 9(c), the ionization occurs around the pulse peak. As the laser intensity is enhanced, the THz radiation will be strengthened since the ionization positions ψ_0 are not varied and $|A(\psi_0)|$ and ω_p grow monotonically. When the laser intensity is high enough to ionize the gas completely, the ionization positions will shift from the pulse peak towards the pulse rising edge, as can be observed in Figs. 9(b) and 9(d). Thus, the laser intensity actually experienced by newly created electrons is not increased. Hence, $|A(\psi_0)|$ as well as ω_p will not grow with the increasing laser intensity and thus saturation can arise.

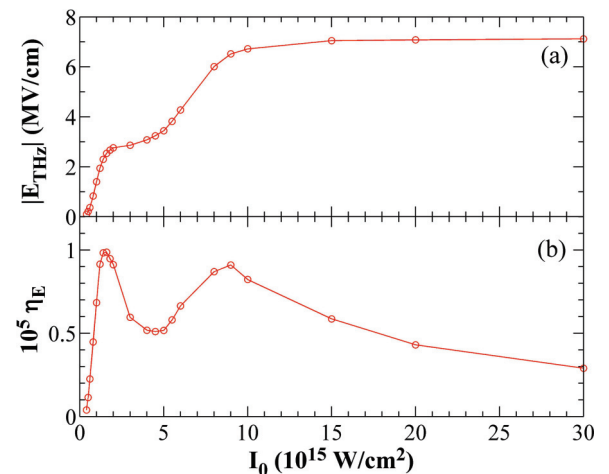


FIG. 7. (Color online) (a) Amplitudes of THz electric fields versus intensities of the main lasers. (b) Energy conversion efficiencies of THz radiation versus intensities of the main lasers. Helium with a gas density of $6.1 \times 10^{17} \text{ cm}^{-3}$ is taken.

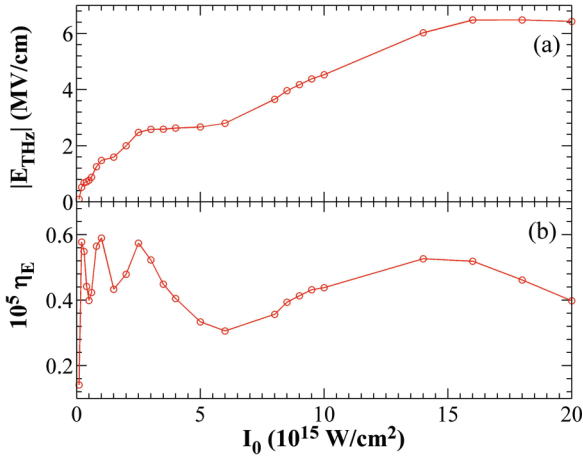


FIG. 8. (Color online) (a) Amplitudes of THz electric fields versus intensities of the main lasers. (b) Energy conversion efficiencies of THz radiation versus intensities of the main lasers. Nitrogen with a gas density of $1.2 \times 10^{17} \text{ cm}^{-3}$ is taken.

Note that Kim *et al.* [14] attributed the saturation to strong THz absorption in a long gas plasma. In our simulations a very short gas plasma (140 μm long) has been taken (the simulation parameters and setup can be seen in the Appendix), which excludes the effect of the gas and plasma absorption of the THz radiation. Therefore, the current investigation presents another possible explanation of this saturation. It should be pointed out that the simulation result in our other paper [16] showed an oscillatory dependence of the THz strength on the laser intensity. The difference comes from two points. First, $\theta = \pi/2$ was taken in Ref. [16] while $\theta = 0$ is used in Figs. 6–8. We had considered that the CE phases have no effect and therefore took the same relative phase as in Ref. [14] but different CE phases, in order to achieve high THz yield efficiency. Second, different temporal wave forms of lasers and durations are taken. A Gaussian wave form is employed here but a \sin^2 wave form in Ref. [16]. The full width at half maximum (FWHM) duration of 50 fs is taken here while it is 12 fs in Ref. [16]. We study the effect of the duration and find that the saturation disappears and an oscillatory behavior starts

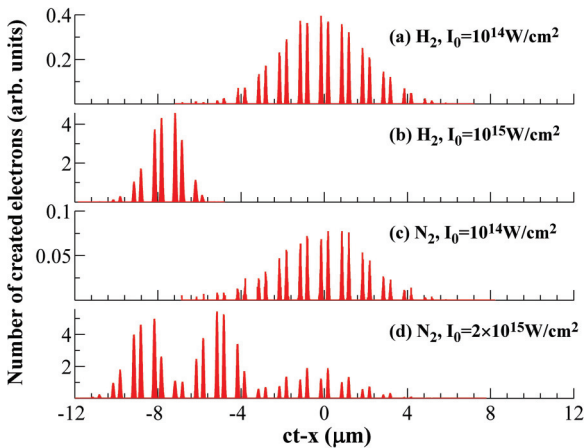


FIG. 9. (Color online) Number distributions of newly created electrons vs $ct - x$, where different gases and different intensities of the main lasers are taken.

to appear when the FWHM duration is decreased to about 10 fs. With a short enough duration, laser ionization occurs at fewer points and cycles and the shift of the ionization position away from the pulse peak tends to be discontinuous with increasing laser intensity. A detailed discussion of this extreme case will be presented elsewhere since the laser duration used in THz experiments is usually longer than 10 fs.

From Figs. 6(a), 7(a), and 8(a), the laser intensity threshold I_s for the saturation can be read for hydrogen, helium, and nitrogen, respectively. The thresholds are about 3×10^{14} , 10^{16} , and $1.6 \times 10^{16} \text{ W/cm}^2$, respectively. Actually, when $I_0 \leq 5 \times 10^{17} \text{ W/cm}^2$ (which is the highest laser intensity taken in our simulations), there are five I_s 's for nitrogen, which correspond to the first to fifth orders of ionization, respectively. In Fig. 8(a) one can clearly see two saturation regions, one between 2.5×10^{15} and $6 \times 10^{15} \text{ W/cm}^2$ and the other around $1.6 \times 10^{16} \text{ W/cm}^2$, due to large differences between the third ionization potential and the fourth one as well as between the fifth one and the sixth one for nitrogen. For helium, two saturation regions are also observed in the curve in Fig. 7(a). The curves in Fig. 6(a) show one saturation plateau only for hydrogen.

One can compare the saturation strengths of the THz radiation generated from the three gases according to I_s . Considering that the THz strength is linearly proportional to $\sqrt{n_e}$ in terms of Eq. (11), we here take gas densities such that hydrogen, helium, and nitrogen are completely ionized to have the same n_e at the highest laser intensity of $5 \times 10^{17} \text{ W/cm}^2$, where the nitrogen can experience complete ionization at the fifth order. Then the THz strength $E_{\text{THz},s}$ at saturation depends on $A(\psi_0)$ only, according to Eq. (11). Because $A(\psi_0) \propto \sqrt{I_s}$, $E_{\text{THz},s}$ should be proportional to $\sqrt{I_s}$. Using the values of $E_{\text{THz},s} = 1.5 \text{ MV/cm}$ and $I_s = 3 \times 10^{14} \text{ W/cm}^2$ of hydrogen, one obtains the saturation strength of the THz radiation at 10 THz from an arbitrary gas as

$$E_{\text{THz},s} = \sqrt{\frac{I_s}{3 \times 10^{14} \text{ W/cm}^2}} \times 1.5 \text{ MV/cm}. \quad (13)$$

In terms of this scaling law and the values of I_s for helium and nitrogen observed in our simulations, one calculates $E_{\text{THz},s} = 8.6$ and 10.9 MV/cm , respectively, for helium and nitrogen. The calculated $E_{\text{THz},s}$ are somewhat larger than those (7.0 and 6.5 MV/cm) obtained from Figs. 7(a) and 8(a). The reason can be found from Fig. 9(d). One can see that the ionization appears at three positions, among which the first two on the left correspond to complete ionization of the first two orders and the third one corresponds to partial ionization of the third order. For a lower order of ionization, the ionization position is farther away from the laser peak and the corresponding laser field and the $A(\psi_0)$ are lower than those of a higher order of ionization. Therefore, for gases composed of more complex atoms, the THz saturation strengths are overestimated more by Eq. (13).

We change gas densities n_{gas} in PIC simulations and find that the THz strength is linearly proportional to $\sqrt{n_{\text{gas}}}$. One example is demonstrated in Fig. 6(a), where the n_{gas} of the red curve is 11.1 times that of the green curve (after complete gas ionization, the red curve with open circles corresponds to $\omega_p/2\pi = 10 \text{ THz}$ and the green curve with solid circles to

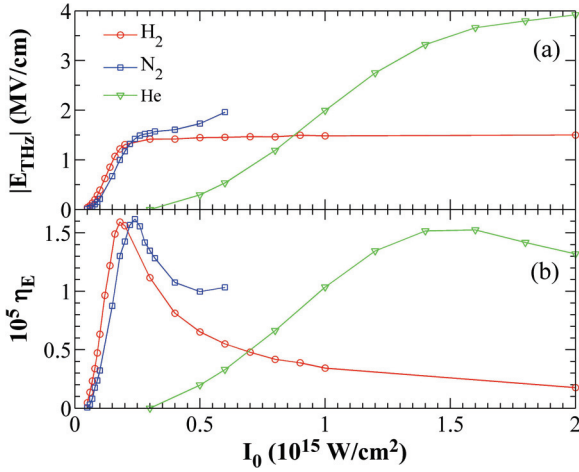


FIG. 10. (Color online) (a) Amplitudes of THz electric fields versus intensities of the main lasers. (b) Energy conversion efficiencies of THz radiation versus intensities of the main lasers. Different curves correspond to hydrogen, helium, and nitrogen with the same atom density of $1.2 \times 10^{18} \text{ cm}^{-3}$.

$\omega_p/2\pi = 3 \text{ THz}$). We have multiplied the THz strengths in the green curve by 3.333. One can see that the two curves almost coincide, which indicates a linear dependence of the THz strength on $\sqrt{n_{\text{gas}}}$ or ω_p . This is because ψ_0 and the resulting $A(\psi_0)$ do not vary with the gas density and the THz strength is determined only by ω_p according to Eq. (11). As a result, through multiplication by a constant, the simulation results presented in Figs. 6(a), 7(a), and 8(a) can be applied to the case with an arbitrary gas density or any THz frequency when the same laser intensity and the same kind of gas are used. With this result, Eq. (13) can also be extended to any gas density or any THz frequency, i.e.,

$$E_{\text{THz},s} = \sqrt{\frac{I_s}{10^{14} \text{ W cm}^{-2}} \frac{n_e}{10^{18} \text{ cm}^{-3}}} \times 0.79 \text{ MV/cm}, \quad (14)$$

where n_e is the plasma electron density after gas ionization. Equation (14) [also Eq. (13)] is applicable to any kind of gas and particularly accurate for the first order of complete ionization of the gas. For instance, for the first order of complete ionization of helium, $E_{\text{THz},s}$ is 2.7 MV/cm observed at $I_s = 1.8 \times 10^{15} \text{ W/cm}^2$ in Fig. 7(a), which is in good agreement with the value 2.74 MV/cm calculated by Eq. (14). A doubled density of helium is taken in Fig. 10(a) and one sees that the corresponding $E_{\text{THz},s}$ is 3.8 MV/cm at $1.8 \times 10^{15} \text{ W/cm}^2$ and the calculated value is 3.7 MV/cm. For the first order of complete ionization of nitrogen, the calculated values also accord well with the simulation results shown in Figs. 8(a) and 10(a). It is interesting to compare Eq. (14) with the simulation results in the range 2.5×10^{15} to $6 \times 10^{15} \text{ W/cm}^2$ displayed in Fig. 8(a), where an obvious saturation plateau appears; this laser intensity range can usually be reached in current THz experiments. The observed THz saturation strength is $E_{\text{THz},s} = 2.6 \text{ MV/cm}$ at $I_s = 2.5 \times 10^{15} \text{ W/cm}^2$, which corresponds to the third order of complete ionization. This approximately agrees with the calculated value 3.35 MV/cm.

We also present the energy conversion efficiency η_E from the two laser pulses to a THz pulse in Figs. 6(b), 7(b), and 8(b). Here, we take the THz radiation energy contained in

the first cycle as the total energy of the THz pulse and apply a THz pulse with almost the same spot size as the drive laser, as observed in our simulations. One observes that peaks of the conversion efficiency appear just at the starting points of the THz strength saturation regions. There are one, two, and five peaks for hydrogen, helium, and nitrogen, respectively, where the fourth peak at about $9 \times 10^{15} \text{ W/cm}^2$ for nitrogen is not obvious due to the small difference between the fourth and fifth orders' ionization potentials. In particular, the efficiency peak for hydrogen is up to 1.6×10^{-5} . Scaling of the conversion efficiency is easily achieved if the same kind of gas is employed. As mentioned previously, the THz strength is linearly proportional to the square root of the gas density n_{gas} and the THz cycle length (or the THz pulse duration) is inversely proportional to ω_p or $\sqrt{n_{\text{gas}}}$. Therefore, for a given kind of gas the conversion efficiency η_E satisfies

$$\eta_E \propto \sqrt{n_{\text{gas}}}. \quad (15)$$

The efficiency peaks for different kinds of gases can be approximately estimated by Eq. (14) as

$$\eta_{E,\text{peak}} = \sqrt{\frac{n_e}{1.2 \times 10^{18} \text{ cm}^{-3}}} \times 1.6 \times 10^{-5}. \quad (16)$$

Equation (16) indicates that the efficiency peaks of the different kinds of gases depend on the plasma electron density only. This is accurate for the first order of complete ionization of gas, as shown in Fig. 10, where the hydrogen, helium, and nitrogen are taken with the same atom density. However, for higher orders of complete ionization of gases, the efficiency peaks are overestimated by Eq. (16) due to the overestimation of $E_{\text{THz},s}$ by Eq. (14). It should be pointed out that η_E can be enhanced further providing shorter laser pulses are used. In our simulations we have taken the laser duration as 50 fs.

We summarize this section briefly. By applying the first order of complete ionization of any kind of gas, one can achieve the same highest energy conversion efficiency to THz radiation at a given frequency. One can obtain a stronger THz radiation at a given frequency through using a gas with higher ionization potential, which has a higher laser intensity threshold for saturation of the THz strength. Therefore, to get stronger THz radiation with the highest conversion efficiency, one can take a gas with a higher first order ionization potential, e.g., helium.

V. EFFECT OF THE SECOND LASER INTENSITY

In Secs. II–IV, we have taken the second laser intensity to be 25% of the main laser intensity in our simulations, i.e., $a_2 = 0.5a_0$. In this section, we study the dependence of the THz generation on the second laser intensity. According to the discussion above, ionization occurs around such a ψ_0 that $\frac{\partial E}{\partial \psi}(\psi_0) = 0$. Taking the derivative of $\frac{\partial E}{\partial \psi}(\psi_0) = 0$ with respect to a_2 , one gets

$$\frac{\partial \psi_0}{\partial a_2} = \frac{\cos(\psi_0)}{a_2 \frac{\partial^2 E}{\partial \psi^2}(\psi_0)}. \quad (17)$$

We consider a small m and the case with $\theta = 0$, which can produce THz radiation efficiently. We here take $m = 2$ as an example to analyze. According to the analysis in Sec. II, one maximum of E appears at $[0, \pi/2]$ and the other appears symmetrically at $[3\pi/2, 2\pi]$, which can also be seen in Figs. 2

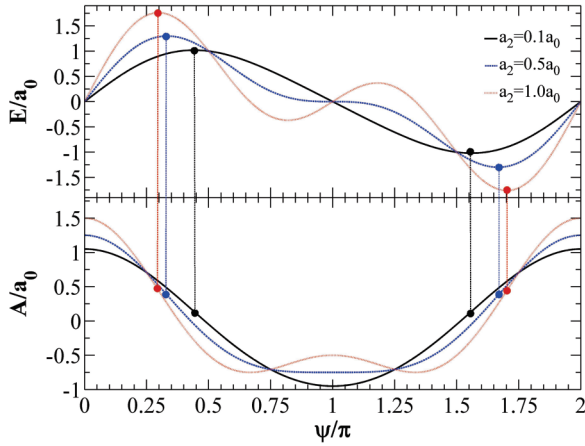


FIG. 11. (Color online) Numerical calculations of Eqs. (1) and (2) with different a_2 , where $\omega_2 = 2\omega_0$ and $\theta = 0$. The solid circles mark the maxima and minima of the electric field E of the mixed lasers and the corresponding values of A .

and 11. Due to the symmetry, one needs to analyze only the dependence of the maximum at $[0, \pi/2]$ on a_2 . At this point, $\cos(\psi_0) > 0$, $\frac{\partial^2 E}{\partial \psi^2}(\psi_0) < 0$, and the resulting $\partial \psi_0 / \partial a_2 < 0$, which implies that ψ_0 drifts away from $\pi/2$ with growth of a_2 (see Fig. 11). Hence, $A(\psi_0)$ increases with increasing a_2 according to Eq. (7) (also see Fig. 11) and the THz radiation is enhanced. This prediction is verified by Fig. 12 when a_2 is not large. In Fig. 13 one also observes that with growing a_2 , the ionization position ψ_0 drifts away from $\pi/2$ within a local laser cycle; the blue vertical line marks the ionization position for the case of $a_2 = 0.1a_0$. In addition, a shift of all the ionization positions away from the laser pulse peak is seen as a_2 increases. Such shift causes a decrease of the laser intensity actually experienced by newly created electrons. This is unfavorable for enhancement of the THz intensity. This negative effect combined with the positive effect of the local drift of ψ_0 away from $\pi/2$ leads to the appearance of the peak shown in Fig. 12. The peak is at about $a_2/a_0 = 1.0$ and 0.6 , respectively, for the main laser intensities of 10^{14} and 10^{15} W/cm². The difference between the two peak positions is because complete ionization

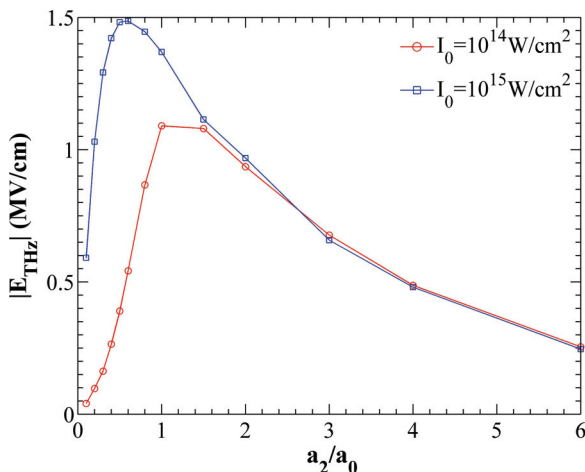


FIG. 12. (Color online) Amplitudes of the THz electric fields versus the ratio of the two laser field amplitudes.

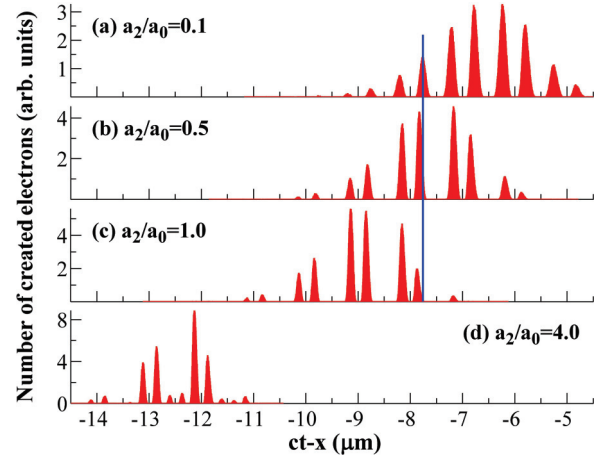


FIG. 13. (Color online) Number distributions of newly created electrons vs $ct - x$, where different ratios of the two laser field amplitude are taken. The blue solid line marks the maximum of the electric fields of the lasers with $a_2/a_0 = 0.1$. The intensities of the main lasers are fixed as 10^{15} W/cm².

appears at a larger a_2 for the lower laser intensity. An additional effect is also found from Eq. (17) as $|\partial \psi_0 / \partial a_2| \propto 1/a_2$, which causes a decrease of the increase of the THz intensity with growing a_2 .

VI. THz SATURATION STRENGTHS AT DIFFERENT INTENSITY RATIOS

We have presented the saturation strength of THz radiation in Eqs. (13) and (14) when $a_2/a_0 = 0.5$ or $I_2/I_0 = 0.25$, where I_2 is the second laser intensity. For experiments and applications, it is interesting to investigate the impact of I_2/I_0 on the THz saturation strength. The THz saturation strength $E_{\text{THz},s}$ versus I_2/I_0 obtained from our simulations is shown in Table I. We get $E_{\text{THz},s}$ by use of a main laser with intensity at or slightly higher than the threshold intensity I_s , where I_s is 3×10^{14} , 10^{16} , and 1.6×10^{16} W/cm², respectively, for hydrogen, helium, and nitrogen, as presented in Sec. IV. Considering that the second laser is weaker or much weaker than the main laser in practical experiments [10–14,20,21], we take I_2/I_0 within 5%–50% in our simulations. One can see from Table I that $E_{\text{THz},s}$ is nearly the same when I_2/I_0 within 20%–50%. This suggests that Eqs. (13) and (14) obtained for $I_2/I_0 = 25\%$ also hold for other I_2/I_0 values between 20% and 50%. $E_{\text{THz},s}$ decreases by about 10% and 25% when I_2/I_0 is

TABLE I. Saturation strengths (MV/cm) of the THz radiation at 10 THz generated from hydrogen (H₂), helium (He), and nitrogen (N₂), respectively, with different laser intensity ratios.

I_2/I_0	$E_{\text{THz},s}^{\text{H}_2}$	$E_{\text{THz},s}^{\text{He}}$	$E_{\text{THz},s}^{\text{N}_2}$
5%	1.12	5.18	5.05
10%	1.36	6.26	5.88
20%	1.49	6.88	6.47
30%	1.51	7.05	6.52
40%	1.51	7.03	6.47
50%	1.53	6.97	6.40

changed to 10% and 5%, respectively, and therefore Eqs. (13) and (14) can be applied through use of a multiplying factor of 0.9 and 0.75 for $I_2/I_0 = 10\%$ and $I_2/I_0 = 5\%$, respectively. Furthermore, Table I shows the results for the THz radiation at 10 THz and it can be applied to any THz frequency by multiplication by a constant.

VII. SUMMARY

In summary, we have studied THz generation in the two-color laser scheme when the second laser takes the frequency of an arbitrary harmonic of the main laser. We have found that the THz radiation is not generated when the second laser is at an odd harmonic frequency and it can be generated only when the laser is at an even harmonic frequency. As the harmonic order increases, the THz yield efficiency decreases, i.e., the highest efficiency is achieved with the second harmonic.

The THz strength depends on the CE phases of both the laser pulses, even if their durations are much longer than the main laser cycle. The strength is proportional to $(-1)^{m/2} \cos(\psi_{CE2} - m\psi_{CE1} + \theta)$, where ψ_{CE1} and ψ_{CE2} are the CE phases of the two pulses, θ is their relative phase displacement, and m is the order of an even harmonic. By detecting the dependence of the THz strength on θ , one can determine both ψ_{CE1} and ψ_{CE2} at the same time. This may provide a diagnosis of CE phases even for long laser pulses, such as 100 fs pulses. In particular, for $\psi_{CE1} = \psi_{CE2} = 0$, the strength scales linearly with $\cos(\theta)$ and the dependence is changed to $\sin(\theta)$ for $\psi_{CE1} = \psi_{CE2} = \pi/2$. This can explain two existing experimental results: one shows $\sin(\theta)$ dependence and the other shows $\cos(\theta)$ dependence, which previously seemed inconsistent. These may be obtained due to the different CE phases used in the experiments, which are usually hard to measure for laser pulses with durations of many cycles.

The THz intensity versus the laser intensity depends on the gas species. For hydrogen it shows a monotonic growth region followed by a saturation plateau. The saturation arises when complete ionization occurs, which also corresponds to the maximum energy conversion efficiency. For gases with more ionization levels, e.g., helium and nitrogen, the THz intensity dependence curves show several saturation plateaus, any two of which are connected by a monotonic growth line. In addition, one can obtain stronger THz radiation at a given frequency by use of gases with higher ionization potentials.

The energy conversion efficiency versus the laser intensity is found to scale linearly with the square root of the density of a given gas species. Therefore, the conversion efficiency scaling law found for a certain gas density or a certain THz frequency can be extended to any density or any THz frequency by multiplying by a constant. It is also found that by applying the first order of complete ionization of any kind of gas, one can achieve the same highest conversion efficiency of the THz radiation at a given frequency. Therefore, to get stronger THz radiation with the highest conversion efficiency, one can take a gas species with a higher first order ionization potential, e.g., helium.

Increase in the second laser intensity leads to a drift of the ionization positions away from the phases of $\pi/2$ or $3\pi/2$ in a

local main laser cycle, which enhances the THz strength. This works only when the second laser intensity is not too high. Otherwise, all ionization positions will shift away from the laser pulse peak, which causes a decrease of the laser intensity actually experienced by newly created electrons. Due to the two effects, an optimum intensity of the second laser for the strongest THz radiation appears.

Scaling of the THz strength with the intensities of the two-color lasers found in our simulations (e.g., Figs. 6–8) indicates that the THz generation discussed here cannot be described simply by the standard nonlinear dielectric polarization in optical media through frequency mixing processes.

ACKNOWLEDGMENTS

This work is supported in part by the National Science Foundation of China (Grants No. 11105217, No. 11121504, No. 11129503, and No. 10925421).

APPENDIX: PARAMETERS AND SETUP OF PIC SIMULATIONS

The simulations are performed using our two-dimensional PIC code developed based upon Refs. [34–37]. In this code, the field ionization of gases is included according to the Ammosov-Delone-Krainov formula [38]. The main laser wavelength is fixed at 1 μm and the second laser frequency is taken as the main laser harmonic. The two laser pulses propagate along the $+x$ direction. They are linearly polarized along the y direction with the electric fields $E = \exp(-\xi^2/\tau_0^2 - y^2/r_0^2)[a_0 \sin(\omega_0\xi) + a_2 \sin(\omega_2\xi + \theta)]$, where $\xi = t - x/c$, $r_0 = 100 \mu\text{m}$, and $\tau_0 = 30$ fs (the full width at half maximum duration is 50 fs). A gas slab with a uniform density profile is distributed between $x = 320 \mu\text{m}$ and $x = 460 \mu\text{m}$. The resolution in the laser propagation direction is 0.01 μm . The resolution in the transverse direction is 0.1 μm . Nine particles per cell are used. We take $\omega_2 = 2\omega_0$, $\theta = 0$, $a_2 = 0.5a_0$, and hydrogen with the density of $6.1 \times 10^{17} \text{ cm}^{-3}$ as the standard simulation parameters, unless otherwise specified.

The PIC simulation results on THz strengths are obtained from the temporal wave forms of the THz pulses propagating along the $-x$ direction in the vacuum, where the detection point is at 10 μm away from the left vacuum-gas boundary. Similar results can be achieved from the THz pulses propagating along the $+x$ direction since a short enough gas length of 140 μm (a few plasma wavelengths) is used. The reason that we use the data of the THz pulses propagating along the $-x$ direction is as follows. The strength of the THz pulse propagating along the $+x$ direction depends on the gas length due to laser and THz absorption and propagation effects [39]. However, the strength of the pulse propagating along the $-x$ direction does not vary with gas length providing it is longer than half of a plasma wavelength [32,40].

We do not present here the temporal wave form of the THz radiation obtained from our simulations. The THz radiation has a near single cycle wave form with the central frequency of ω_p , which is almost unchanged with different laser parameters and gas species. One can see such wave forms in Refs. [16–18,32,33].

- [1] D. You, R. R. Jones, P. H. Bucksbaum, and D. R. Dykaar, *Opt. Lett.* **18**, 290 (1993).
- [2] E. Budiarto, J. Margolies, S. Jeong, J. Son, and J. Bokor, *IEEE J. Quantum Electron.* **32**, 1839 (1996).
- [3] H. Hamster, A. Sullivan, S. Gordon, W. White, and R. W. Falcone, *Phys. Rev. Lett.* **71**, 2725 (1993).
- [4] H. Hamster, A. Sullivan, S. Gordon, and R. W. Falcone, *Phys. Rev. E* **49**, 671 (1994).
- [5] A. Sagiska, H. Daido, S. Nashima, S. Orimo, K. Ogura, M. Mori, A. Yogo, J. Ma, I. Daito, A. S. Pirozhkov, S. V. Bulanov, T. Zh. Esirhepov, K. Shimizu, and M. Hosoda, *Appl. Phys. B: Lasers Opt.* **90**, 373 (2008).
- [6] Y. Gao, T. Drake, Z. Chen, and M. F. DeCamp, *Opt. Lett.* **33**, 2776 (2008).
- [7] C. Li, M.-L. Zhou, W.-J. Ding, F. Du, F. Liu, Y.-T. Li, W.-M. Wang, Z.-M. Sheng, J.-L. Ma, L.-M. Chen, X. Lu, Q.-L. Dong, Z.-H. Wang, Z. Lou, S.-C. Shi, Z.-Y. Wei, and J. Zhang, *Phys. Rev. E* **84**, 036405 (2011).
- [8] Y. T. Li, C. Li, M. L. Zhou, W. M. Wang, F. Du, W. J. Ding, X. X. Lin, F. Liu, Z. M. Sheng, X. Y. Peng, L. M. Chen, J. L. Ma, X. Lu, Z. H. Wang, Z. Y. Wei, and J. Zhang, *Appl. Phys. Lett.* **100**, 254101 (2012).
- [9] W. P. Leemans, C. G. R. Geddes, J. Faure, C. Tóth, J. van Tilborg, C. B. Schroeder, E. Esarey, G. Fubiani, D. Auerbach, B. Marcellis, M. A. Carnahan, R. A. Kaindl, J. Byrd, and M. C. Martin, *Phys. Rev. Lett.* **91**, 074802 (2003).
- [10] D. J. Cook and R. M. Hochstrasser, *Opt. Lett.* **25**, 1210 (2000).
- [11] M. Kress, T. Löffler, S. Eden, M. Thomson, and H. G. Roskos, *Opt. Lett.* **29**, 1120 (2004).
- [12] T. Bartel, P. Gaal, K. Reimann, M. Woerner, and T. Elsaesser, *Opt. Lett.* **30**, 2805 (2005).
- [13] X. Xie, J. Dai, and X.-C. Zhang, *Phys. Rev. Lett.* **96**, 075005 (2006).
- [14] K. Y. Kim, J. H. Glowina, A. J. Taylor, and G. Rodriguez, *Opt. Express* **15**, 4577 (2007).
- [15] H. C. Wu, J. Meyer-ter-Vehn, and Z. M. Sheng, *New J. Phys.* **10**, 043001 (2008).
- [16] W.-M. Wang, Z.-M. Sheng, H.-C. Wu, M. Chen, C. Li, J. Zhang, and K. Mima, *Opt. Express* **16**, 16999 (2008).
- [17] W.-M. Wang, S. Kawata, Z.-M. Sheng, Y.-T. Li, and J. Zhang, *Phys. Plasmas* **18**, 073108 (2011).
- [18] W.-M. Wang, Z.-M. Sheng, Y.-T. Li, L. M. Chen, Q.-L. Dong, X. Lu, J.-L. Ma, and J. Zhang, *Chin. Opt. Lett.* **9**, 110002 (2011).
- [19] M. Chen, A. Pukhov, X.-Y. Peng, and O. Willi, *Phys. Rev. E* **78**, 046406 (2008).
- [20] X.-Y. Peng, C. Li, M. Chen, T. Toncian, R. Jung, O. Willi, Y.-T. Li, W.-M. Wang, S.-J. Wang, F. Liu, A. Pukhov, Z.-M. Sheng, and J. Zhang, *Appl. Phys. Lett.* **94**, 101502 (2009).
- [21] X.-Y. Peng, R. Jung, T. Toncian, O. Willi, and J.-Hu. Teng, *Appl. Phys. Lett.* **94**, 221107 (2009).
- [22] I. Babushkin, W. Kuehn, C. Kohler, S. Skupin, L. Berge, K. Reimann, M. Woerner, J. Herrmann, and T. Elsaesser, *Phys. Rev. Lett.* **105**, 053903 (2010).
- [23] H. W. Du, M. Chen, Z. M. Sheng, and J. Zhang, *Laser Part. Beams* **29**, 447 (2011).
- [24] Z.-M. Sheng, K. Mima, J. Zhang, and H. Sanuki, *Phys. Rev. Lett.* **94**, 095003 (2005).
- [25] Z.-M. Sheng, K. Mima, and J. Zhang, *Phys. Plasmas* **12**, 123103 (2005).
- [26] Z.-M. Sheng, H.-C. Wu, K. Li, and J. Zhang, *Phys. Rev. E* **69**, 025401(R) (2004).
- [27] H.-C. Wu, Z.-M. Sheng, and J. Zhang, *Phys. Rev. E* **77**, 046405 (2008).
- [28] X. G. Dong, Z. M. Sheng, H. C. Wu, W. M. Wang, and J. Zhang, *Phys. Rev. E* **79**, 046411 (2009).
- [29] C. D'Amico, A. Houard, M. Franco, B. Prade, A. Mysyrowicz, A. Couairon, and V. T. Tikhonchuk, *Phys. Rev. Lett.* **98**, 235002 (2007).
- [30] Y. Liu, A. Houard, B. Prade, S. Akturk, A. Mysyrowicz, and V. T. Tikhonchuk, *Phys. Rev. Lett.* **99**, 135002 (2007).
- [31] A. Houard, Y. Liu, B. Prade, V. T. Tikhonchuk, and A. Mysyrowicz, *Phys. Rev. Lett.* **100**, 255006 (2008).
- [32] W.-M. Wang, Z.-M. Sheng, X.-G. Dong, H.-W. Du, Y.-T. Li, and J. Zhang, *J. Appl. Phys.* **107**, 023113 (2010).
- [33] W.-M. Wang, S. Kawata, Z.-M. Sheng, Y.-T. Li, J. Zhang, L. M. Chen, L. J. Qian, and J. Zhang, *Opt. Lett.* **36**, 2608 (2011).
- [34] C. K. Birdsall and A. B. Langdon, *Plasma Physics via Computer Simulation* (McGraw-Hill, New York, 1985).
- [35] R. W. Hockney and J. W. Eastwood, *Computer Simulation Using Particles* (McGraw-Hill, New York, 1981).
- [36] J. W. Eastwood, *Comput. Phys. Commun.* **64**, 252 (1991).
- [37] T. Umeda, Y. Omura, T. Tominaga, and H. Matsumoto, *Comput. Phys. Commun.* **156**, 73 (2003).
- [38] M. V. Ammosov, N. B. Delone, and V. P. Krainov, *Sov. Phys. JETP* **64**, 1191 (1986).
- [39] Y. Liu, A. Houard, M. Durand, B. Prade, and A. Mysyrowicz, *Opt. Express* **17**, 11480 (2009).
- [40] W.-M. Wang, Ph.D. thesis, Institute of Physics, Chinese Academy of Sciences, 2009.